Heat transfer measurements with TOIRT method

S. Solnař, K. Petera, M. Dostál, T. Jirout

Czech technical university in Prague, Faculty of Mechanical Engineering, Department of Process Engineering

Received: date / Revised version: date

Abstract. Temperature Oscillation Infra-Red Thermography (TOIRT) method was used to measure heat transfer coefficients between a flat surface and a confined impinging jet generated by an impeller in a difusor and baffled vessel. The TOIRT method is based on measuring a phase-lag between the oscillating heat flux applied to the heat transfer surface and the surface temperature response using a contactless infra-red camera. The phase lag is in a direct relationship with the heat transfer coefficient.

1 Introduction

Within the technical progress we try among the other things to maximize heat transfer in the apparatuses in which heat transfer happens. The intensity of convective heat transfer is characterized by the size of the heat transfer coefficient α which can be found in Newton's law

$$\dot{Q} = \alpha\, S\, \Delta T, \tag{1}$$

where $\dot{Q}$ is convective heat flux, S heat transfer surface and ΔT temperature difference between surface and surroundings.

There are two main groups of heat transfer measuring methods: time dependent (where the temperature time response is measured) and time independent (where the system is in thermodynamic equilibrium and the heat flux is measured). TOIRT method stands somewhere between these two groups.

TOIRT method was used by S. Freund [1] to measure the temperature response of wall which was heated by an oscillating heat flux. In this work author also measured heat transfer coefficients of various geometries like impinging jet falling to flat surface or water flow in tube. Another usage of TOIRT method [2] measured the heat transfer coefficients of falling water to water level.

Experimental data given by this method show very good agreement with data measured by conventional methods.

2 Temperature oscillation method

The principle of Wandelt and Roetzel's TOIRT method [3] is shown on Fig. 1. The method is based on measuring the temperature field on the wall with IR camera. Temperature field depends on two main factors: modulated heat flux and heat transfer coefficients on both sides of the wall with the thickness δ. The oscillating heat flux is modulated by the sine function and the temperature response is also a sine function. An information that we are trying to find is phase lag between these two sine functions.

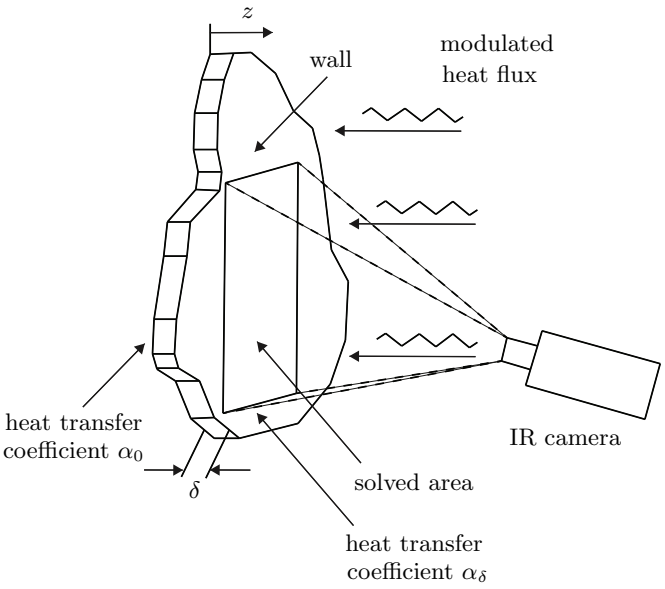

Fig. 1: The principle of Wandelt and Roetzel's method [3]

Time change of a temperature of a homogeneous wall (defined by temperature conductivity a) is described by Fourier's equation

$$\frac{\partial T}{\partial t} = a\left(\cancel{\frac{\partial^2 T}{\partial x^2}} + \cancel{\frac{\partial^2 T}{\partial y^2}} + \frac{\partial^2 T}{\partial z^2}\right). \tag{2}$$

While neglecting the lateral heat conduction in the wall (first two partial derivations on right side) it is possible to find an analytical solution in the case of periodical oscillation of heat flux. The boundary conditions are of the

third kind (Newton's) and can be written as

$$\lambda \left.\frac{\partial T}{\partial z}\right|_{\mathrm{z=0}} = \alpha_0 \, T|_{\mathrm{z=0}} \ , \tag{3}$$

$$\lambda \left.\frac{\partial T}{\partial z}\right|_{\mathrm{z=d}} = \hat{q} \sin \omega t - \alpha_\delta \, T|_{\mathrm{z=\delta}}, \tag{4}$$

where α_0 is heat transfer coefficient we are looking for, α_δ heat transfer coefficient on the other side, ω angular speed of oscillating heat flux and $\hat{q}$ amplitude of heat flux. Authors used a Laplace transformation for solving this system of equations and found solution

$$T(z,t) = A(z) \, \sin(\omega \, t - \varphi(z)). \tag{5}$$

The phase-lag $\varphi(z)$ on the surface with periodic oscillating heat flux can be written as

$$\tan \varphi|_{\mathrm{z=\delta}} = \frac{c_1 + 2\xi\psi_0 c_2 + 2\xi^2\psi_0^2 c_3}{2\xi\psi_0(1+r)c_0 + 2\xi^2\psi_0^2(1+2r)c_1 + 4\xi^3\psi_0^3 r c_2 + c_3} \tag{6}$$

where dimensionless parameters r, ψ_0, ξ and $c_{0,1,2,3}$ are

$$r = \frac{\alpha_\delta}{\alpha_0}, \quad \psi_0 = \frac{\alpha_0 a}{\delta \lambda \omega}, \quad \xi = \delta \sqrt{\frac{\omega}{2a}} \tag{7}$$

$$\begin{aligned} c_0 &= \cosh^2 \xi \cos^2 \xi + \sinh^2 \xi \sin^2 \xi \\ c_1 &= \cosh \xi \sinh \xi + \cos \xi \sin \xi \\ c_2 &= \cosh^2 \xi \sin^2 \xi + \sinh^2 \xi \cos^2 \xi \\ c_3 &= \cosh \xi \sinh \xi - \cos \xi \sin \xi \end{aligned} \tag{8}$$

These equations show no dependency on the amplitude of heat flux. On the other hand, experimental results are affected by the precise reading of the time lag between the heat flux and surface temperature.

3 Application of method

For TOIRT method, it is needed to generate sinusoidally modulated heat flux and to monitor temperature fields in precisely defined time intervals. The sine function is modulated in the first channel of function generator BK Precision 4052. The voltage output 1 to 10 V is connected with stabilized power supply and controls halogen lights. The halogen lights are used for generating heat flux, because they have relatively small efficiency, so most of the electric power is transformed to heat. We use four 500W halogen evenly distributed lights so the lateral conduction can be neglected.

Freund [1] wrote that if dimensionless thickness of the wall $\xi < 0.5$, the lateral conduction is negligible compared to the heat transfer rate through the wall and the spatial resolution is then expected to be limited by the resolution of the camera. In our case, the $\xi = 0.114$ therefore we were in accordance with this condition.

Second channel of BK Precision 4052 is used for generating impulses that are used for triggering the IR camera thermo IMAGER TIM 160 with resolution 160×120 points.

The sine heat flux with frequency 0,1 Hz was used in our experiments. Sample frequency of IR camera was 10 Hz.

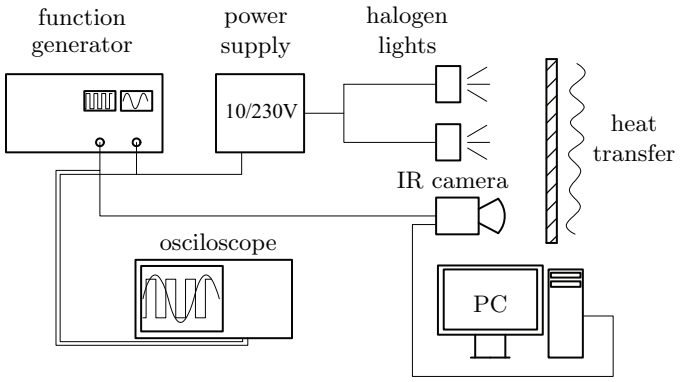

Fig. 2: Wiring schematics

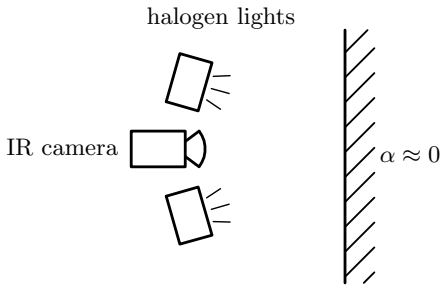

Fig. 3: Time synchronisation

Table 1: Time synchronisation results

	phase-lag (°)	time delay (s)
zero heat transfer method	8.271	0.229
recording method	8.377	0.232

3.1 Time synchronisation

This method is based on precise time measurements so it is necessary to take into account the time delay of measuring system itself. The biggest amount of time delay lies in the halogen lights and their thermal capacity, which has to be overcome when the signal changes.

The first method for time synchronisation measures the same case of experiment but on the semi-infinite body. The schema of time synchonization is on Fig. 3. The semi-infinite body leads to almost zero heat transfer and the measured phase-lag is taken as a sync phase-lag.

The second method records halogen lights at a step change of control voltage with speed camera. The results of time synchronisation are summarized in Tab. 1.

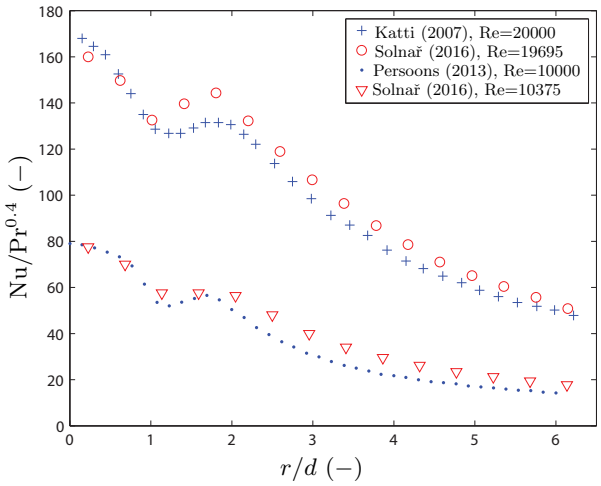

Fig. 4: Results comparsion of impinging jet, $H/D = 1$

4 Validation

The method was validated by results measured on a jet impinging perpendicularly the plate. This geometry was measured many times, see Katti and Prabhu [4] or Persoons et al. [5], for example.

Katti and Prabhu [4] measured the jet impinging perpendicularly the target plate (80×160 mm) made of stainless steel foil with thickness 0.06 mm. Air was supplied by an compressor through a calibrated orifice flow meter and was cooled to the required temperature. The target plate was heated by ohmic heating and thanks to the low thickness the lateral conduction was neglected. The temperature field was measured with IR camera positioned on the other side of target plate. The heat transfer coefficients were established from the temperature time response.

Persoons et al. [5] also measured impinging jet with air, but for lower Reynolds numbers. They used a heat flux sensor which measured the temperature difference across a well-defined thermal barrier. The heat transfer coefficients were determined from measured heat flux.

Our impinging jet experiment was made with water. The jet tube is made of aluminium with inner diameter $d = 22$ mm and corresponding length to $45\,d$. The water circuit is opened above the bottom of unbaffled vessel (diameter $D = 392$ mm). The circuit is powered by a centrifugal water pump with speed control via electric frequency inverter. The pump inlet is connected with the water in the vessel so the height of water level is constant. The pump outlet is connected with the induction flow meter (Krohne OptiFlux 5300). The volumetric flow is used for calculating the mean velocity in the tube and Reynolds numbers according to equation

$$\mathrm{Re} = \frac{u\,d\,\rho}{\mu} \tag{9}$$

where u is mean velocity in tube, ρ water density and μ dynamic viscosity. Temperature of water was measured with Pt1000 platinum ohmic temperature sensor and was 20.5 ± 1.5°C through all the measurings. Corresponding water properties at this temperature are: density $\rho = 998.21\ \mathrm{kg\,m^{-3}}$, dynamic viscosity $\mu = 1,002$ mPa s and Prandtl number 6.98.

5 Experiment setup

Scheme of our experiments is depicted on Fig. 5 and Fig 6. For both experiments an plastic vessel with diameter $D = 392$ mm is used. The bottom of the vessel is made of stainless steel with thickness 0.99 mm and it is coated by a black matt color on the outer side of the vessel bottom.

Thermo-physical properties of the vessel bottom are: heat conductivity $14.6\ \mathrm{W\,m^{-1}\,K^{-1}}$, density $7800\ \mathrm{kg\,m^{-3}}$ and specific heat capacity $501\ \mathrm{J\,kg^{-1}\,K^{-1}}$. The vessel is filled with water to height H. Height h of difusor or impeller above botoom is adjusted with accuracy of 1 mm.

The IR camera was set to monitor temperature fields on the entire bottom of the vessel. The temperature fields were measured with accuracy 0.1°C and spatial resolution about 3.3 mm/pixel.

Temperature of water in the vessel has been measured with Pt1000 platinum ohmic temperature sensor.

5.1 Impeller in difusor

In the first case (Fig. 5 left), an impeller (six-blade, 45°, diameter $d = 61$ mm) in difusor (diameter $d_v = 70$ mm) was measured. Experiments were performed for ratio $h/d_v = 1$. The water level was maintained at $H = D = 392$ mm. Reynolds numbers were calculated according to equation

$$\mathrm{Re} = \frac{n\,d^2\,\rho}{\mu} \tag{10}$$

where n is rotation speed of impeller and d is diameter of the impeller. The water temperature during measurements was 25.2 ± 1.1°C. With corresponding thermophysical properties of water, the Reynolds numbers were from 6 000 to 26 000.

5.2 Impeller in baffled vessel

In the second case (Fig. 5 right), an impeller (six-blade, 45°, diameter $d = 131$ mm) in a baffled (4 baffles $B = 40$ mm) vessel was measured. Experiments were performed for ratio $h/d = 1$. The height of water level was maintained at $H = D = 392$ mm. Reynolds numbers were calculated according to equation (10) and they were within range 17 000 – 95 000. The water temperature during measurements was 24.6 ± 1.8°C.

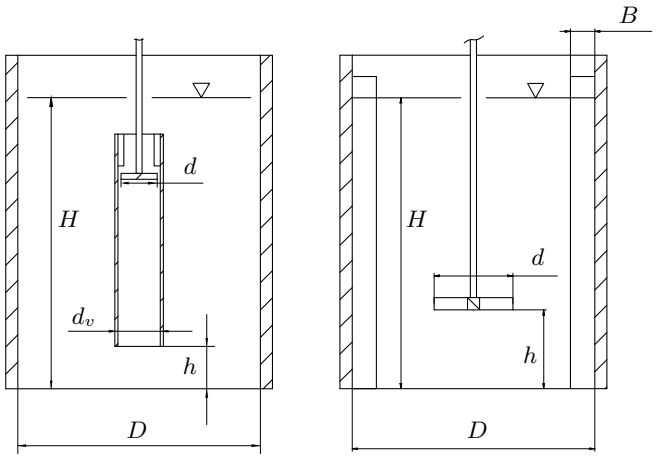

Fig. 5: Drawing of experiments, Left: impeller in difusor, Right: impeller in baffled vessel

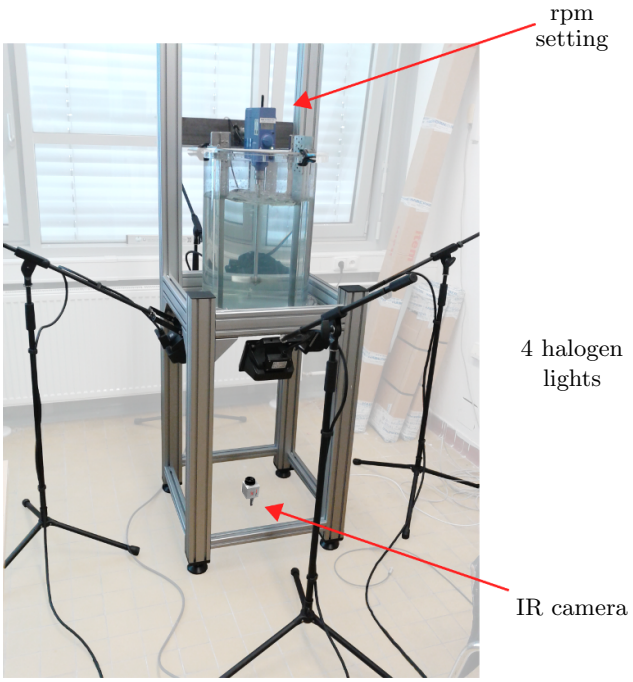

Fig. 6: Experimental setup photo

6 Data reduction

The temperature fields obtained from IR camera are transformed into a 3D matrix (160px × 120px × number of shots) in MATLAB. Time dependence of temperature in points corresponds with sinusoid and exponential function (water in vessel is slowly heated). Wandelt and Roetzel [3] invented the method for steady-state temperature oscillations so the exponential part of time dependence of temperature has to be removed (see Fig. 7).

The phase lags $\varphi(x, y)$ are evaluated by using a nonlinear regression procedure on the revised data. After this procedure, the phase lag from time synchronisation is subtracted and the phase lags $\varphi(x, y)$ are transformed to heat

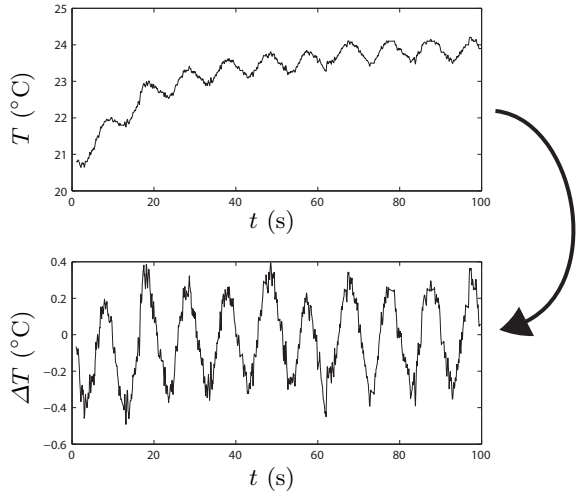

Fig. 7: Example of removing the exponential dependency of measured data

transfer coefficients $\alpha(x, y)$. Nusselt numbers are calculated by

$$\mathrm{Nu} = \frac{\alpha\, d_{\mathrm{char}}}{\lambda} \tag{11}$$

where λ is heat conductivity coefficient and d_{char} is characteristic length (d for impeller in baffled vessel, d_v for difusor). The Nusselt number is then expressed in the form of correlation relationship

$$\frac{\mathrm{Nu}}{\mathrm{Pr}^{0.4}} = C\,\mathrm{Re}^{m} \tag{12}$$

where C is geometric parameter. The Prandtl number has not been investigated in these experiments.

7 Results

Nusselt number dependencies on dimensionless coordinate r/d are on Fig. 8 and Fig. 10. Evaluated parameters of equation (12) are summarized in Tab. 2.

7.1 Impeller in baffled vessel

The distributions of Nusselt number in the case of impeller in a baffled vessel show a visible increase around dimensionless coordinate $r/d \approx 0.5$, but this increase is not very significant. This coordinate coresponds with the end of the impeller blades.

Fig. 9 illustrates a surface graph of heat transfer coefficients. As we can see there are areas with higher intensities of heat transfer due to swirling around baffles. These swirling effects are taken into count in averaged Nusselt number $\overline{\mathrm{Nu}}$.

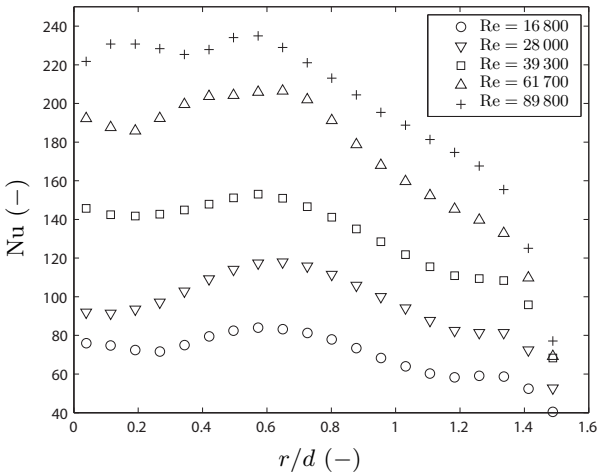

Fig. 8: Nusselt number distribution, impeller in baffled vessel, $h/d = 1$, Pr = 6.98 (water)

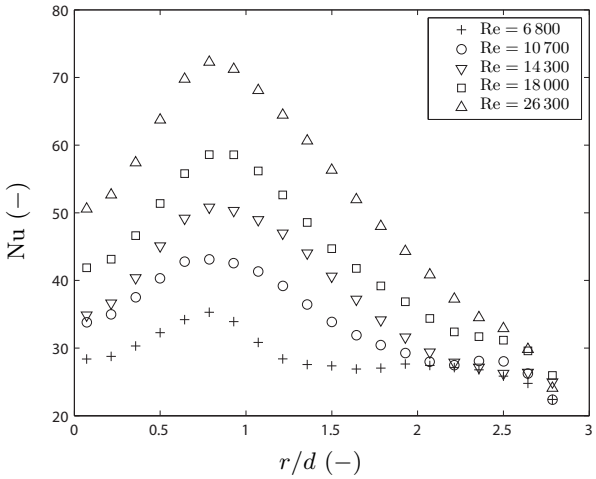

Fig. 10: Nusselt number distribution, difusor, $h/d = 1$, Pr = 6.98 (water)

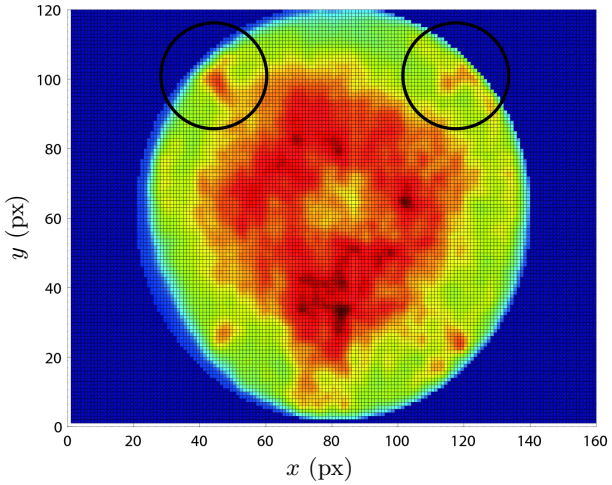

Fig. 9: Intensity of convective heat transfer with highlighted swirling in baffle areas

Table 2: Experimental results in the form of equation (12)

	Impeller in baffled vessel		Impeller in difusor	
	C	m	C	m
Nu_0	0.0907	0.6811	0.5261	0.4487
$\overline{\mathrm{Nu}}$	0.1016	0.5822	0.6466	0.4188

7.2 Impeller in difusor

The distributions of Nusselt number in the case of difusor show significant peaks arround $r/d \approx 0.8$ where it is about 50% higher than the Nusselt number at dimensionless coordinate $r/d = 0$. In this case, we can conclude some similarities between the impinging jet and impeller in difusor. The peak of convective heat transfer in the case of impinging jet is located at dimensionless coordinate about $r/d = 2$. In the case of impeller in difusor, this peak is located at coordinate about $r/d = 1$.

8 Measurement accuracy

This measurement technique has no dependency on the amplitude of heat flux so the minimum of the heat flux is given by a sensitivity of IR camera.

On the other hand, experimental results are affected in time scale. One degree error in the phase-lag (in our case that means: 1 deg = $0.02\overline{7}$ s of time-lag) can cause an error in percent of heat transfer coefficient.

As we can see in (7) results are in a relationship with thermo-physical properties of the wall and with the thickness of the wall. Thermo-physical properties have no significant importance for the results, but the thickness of the wall has. Half a milimeter error in measuring the wall can cause an error in tens of percents of heat transfer coefficient.

9 Conclusion

The TOIRT method was used for heat transfer measuring and results of impinging jet experiments were compared with the literature data to validate the method. Results are in good agreement with both here cited references [4], [5].

Heat transfer coeficients on a flat bottom of a vessel were measured in wide range of Reynolds numbers for two geometries: impeller in baffled vessel and impeller in difusor. In the case of the impeller in baffled vessel, the effect of swirling in baffle areas was found. These swirling effects were taken into count in averaged Nusselt number $\overline{\mathrm{Nu}}$.

In the case of impeller in difusor, similarities with impinging jet falling to flat surface were found. The peak of convective heat transfer in case of impinging jet is located

at dimensionless coordinate about $r/d = 2$. In the case of impeller in difusor this peak is located at coordinate about $r/d = 1$.

Acknowledgment

This work is supported by research project of the Grant Agency of Czech Republic No. 14-18955S.

Nomenclature

a	thermal diffusivity, $a = \lambda/\rho\, c_\mathrm{p}$ ($\mathrm{m^2\,s^{-1}}$)
A	amplitude (-)
B	baffle dimension (m)
C	geometric constant (-)
$c_{0,1,2,3}$	dimensionless parameters
d, D	diameter (m)
d_char	characteristic dimension (m)
d_v	cylinder diameter (m)
h, H	height (m)
m	exponent (-)
n	revolutions ($\mathrm{s^{-1}}$)
Nu	Nusselt number, Nu= $\alpha\, d_\mathrm{char}/\lambda$, (-)
Nu_0	Nusselt number at $r/d = 0$
$\overline{\mathrm{Nu}}$	averaged Nusselt number
Pr	Prandtl number, Pr= $\rho\, c_\mathrm{p}\, \nu/\lambda$ (-)
$\dot{Q}$	heat flux ($\mathrm{W\,m^{-2}}$)
$\hat{q}$	amplitude of heat flux ($\mathrm{W\,m^{-2}}$)
Re	Reynolds number, Re= $n\, d^2\, \rho/\mu = u\, d\, \rho/\mu$ (-)
S	surface ($\mathrm{m^2}$)
t	time (s)
T	temperature (°C)
u	velocity ($\mathrm{m\,s^{-1}}$)
α	heat transfer coefficient ($\mathrm{W\,m^{-2}\,K^{-1}}$)
δ	dimension (m)
λ	heat conductivity ($\mathrm{W\,m^{-1}}$)
μ	dynamic viscosity (Pa s)
ν	kinematic viscosity ($\mathrm{m^2\,s^{-1}}$)
ρ	density ($\mathrm{kg\,m^{-3}}$)
φ	phase lag (°)
ω	annular speed ($\mathrm{s^{-1}}$)
r, ψ_0, ξ	dimensionless parameters (-)

References

1. S. Freund, *Local Heat Transfer Coefficients Measured with Temperature Oscillation IR Thermography* (Hamburg, 2008)
2. S. Freund, A. G. Pautsch, T. A. Shedd, S. Kabelac, International Journal of Heat and Mass Transfer **50**, (2007), p. 1953–1962
3. M. Wandelt and W. Roetzel, Quantitaive Infrared Thermography 96, (1997) p. 189–194
4. V. Katti and S. Prabhu, International Journal of Heat and Mass Transfer **51**, (2008), p. 4480–4495
5. T. Persoons, K. Balgazin, K. Brown, D. B. Murray, Journal of Heat Transfer **135**, (2013)
6. S. Freund, S. Kabelac, International Journal of Heat and Mass Transfer **53**, (2010), p. 3764–3781
7. N. Zuckerman, N. Lior, Advances in Heat Transfer **39**, (2006), p.565–631
8. K. Rehme, *Handbook of single-phase convective heat transfer* (A Wiley-Interscience Publication, 1987)
9. K. W. Treuren, Z. Wang, P. T. Ireland, T. V. Jones, The American society of mechanical engineers **47**, (1993)
10. D. Lytle, B. W. Webb, International Journal of Heat and Mass Transfer **37**, (1994), p. 1687–1697
11. M. Hogler, Advances in Heat Transfer **13**, (1977), p. 1–59
12. R. Viskanta, Experimental Thermal and Fluid Science, (1993), p. 111–134
13. V. V. Katti, S. N. Yasaswy, S. V. Prabhu, Heat and Mass Transfer, (2011), p. 237–244
14. A. Herchang, J. J. Yuh, Y. Jer-Nah, International Journal of Heat and Mass Transfer **45**, (2002), p. 4096–4078